The emergence of lines of hierarchy in collective motion of biological systems

IOP Publishing Phys. Biol. 20 (2023) 055001 https://doi.org/10.1088/1478-3975/acdc79

Physical Biology

OPEN ACCESS

RECEIVED
20 February 2023

REVISED
16 May 2023

ACCEPTED FOR PUBLICATION
7 June 2023

PUBLISHED
29 June 2023

PAPER

The emergence of lines of hierarchy in collective motion of biological systems

James M Greene[1], Eitan Tadmor[2,*] and Ming Zhong[3]

[1] Department of Mathematics, Clarkson University, Potsdam, NY, United States of America
[2] Department of Mathematics and Institute for Physical Science and Technology, University of Maryland, College Park, MD, United States of America
[3] Department of Applied Mathematics, Illinois Institute of Technology, Chicago, IL, United States of America
* Author to whom any correspondence should be addressed.

E-mail: tadmor@umd.edu

Keywords: collective dynamics, emergent behavior, lines of hierarchy, active particles

Abstract

The emergence of large-scale structures in biological systems, and in particular the formation of lines of hierarchy, is observed at many scales, from collections of cells to groups of insects to herds of animals. Motivated by phenomena in chemotaxis and phototaxis, we present a new class of alignment models that exhibit alignment into lines. The spontaneous formation of such 'fingers' can be interpreted as the emergence of leaders and followers in a system of identically interacting agents. Various numerical examples are provided, which demonstrate emergent behaviors similar to the 'fingering' phenomenon observed in some phototaxis and chemotaxis experiments; this phenomenon is generally known to be a challenging pattern for existing models to capture. A novel protocol for pairwise interactions provides a fundamental alignment mechanism by which agents may form lines of hierarchy across a wide range of biological systems.

1. Introduction—emergent phenomena in biological systems

Emergent phenomena in collective dynamics are observed in a wide range of biological systems and across different scales—from cells to bacteria, from insects to fish, from humans to other mammals. Accordingly, it has been a topic of scientific interest in a wide range of disciplines, including biology, ecology, physics, mathematics and computer science [1]. In this context, one is concerned with 'active particles' which consist of living agents (and likewise, certain types of mechanical agents) equipped with senses and sensors with which they probe the environment. These are responsible for small-scale pairwise interactions. The phenomenon of emergence is observed when a crowd of agents, driven by those small-scale interactions, is self-organized into large-scale formations: ants form colonies, insects swarm, birds fly in flocks, mobile networks coordinate a rendezvous or create traffic jams, human opinions evolve into political parties and so on. Thus, with no apparent central control or a built-in bias in the dynamics, the following questions arise: where does this unity from within come from and what is behind the seemingly spontaneous self-organization?

Let $\phi(\mathbf{x}_i, \mathbf{x}_i)$ denote the amplitude of pairwise interaction of agents positioned at $\mathbf{x}_i$ and $\mathbf{x}_j$. Recent studies of collective dynamics have identified different classes of interaction kernels that play a decisive role in governing the different features of their emergent behavior [2–4]. These include metric kernels depending on the metric distance between agents [5, 6]

$$\phi(\mathbf{x}_i, \mathbf{x}_j) = \phi(|\mathbf{x}_i - \mathbf{x}_j|). \tag{1}$$

Then there are topologically based kernels depending on how crowded is the region enclosed between agents positioned at $\mathbf{x}_i$ and $\mathbf{x}_j$, rather than their metric distance [7, 8]

$$\phi(\mathbf{x}_i, \mathbf{x}_j) = \phi\{\#k : \mathbf{x}_k \in \mathcal{C}(\mathbf{x}_i, \mathbf{x}_j)\}. \tag{2}$$

Further, we distinguish between the class of long-range heavy-tailed kernels $\int_0^\infty k(r)\mathrm{d}r = \infty$, expressed in terms of their radial envelope [9, 10]

$$k(r) := \min\{\phi(\mathbf{x}, \mathbf{x}') : |\mathbf{x} - \mathbf{x}'| \leqslant r\}, \tag{3}$$

and singular-headed kernels $k(r) = r^{-\beta}, \beta > 0$ [11–13], versus short range, compactly supported kernels [14] $k(r) \lesssim \mathbb{1}_{r \leqslant r_0}$. Our primary interest is in self-organization that is independent of external forces/stimuli; for a mathematical analysis of the latter see [15], for example.

1.1. Attraction, repulsion, alignment

One can classify three main types of pairwise interactions that govern the emergent phenomena observed in biological systems, namely attraction, repulsion and alignment [16–18]. The first two main features are *attraction*, which acts as a cohesion towards the average position of neighboring agents, and *repulsion*, which steers to avoid collisions. These are familiar from particle dynamics. A typical first-order attraction–repulsion dynamics can be expressed by

$$\dot{\mathbf{x}}_i(t) = -\frac{1}{|\mathcal{N}_i(t)|} \sum_{j \in \mathcal{N}_i(t)} \phi(\mathbf{x}_i, \mathbf{x}_j)(\mathbf{x}_i - \mathbf{x}_j). \quad (4)$$

Here, the agent positioned at $\mathbf{x}_i$ interacts with its neighbors at $\mathcal{N}_i(t) := \{j : \phi(\mathbf{x}_i(t), \mathbf{x}_j(t)) \neq 0\}$, of size $|\mathcal{N}_i|$. Thus, with the pre-factor normalization in (4), it can be interpreted as a local *environmental averaging* of positions. Short-range versus long-range kernels translate into local versus global neighborhoods. Attraction and repulsion are dictated by the positive, respectively negative, parts of $\phi_{ij} = \phi(\mathbf{x}_i, \mathbf{x}_j)$. The balance between attraction and repulsion is responsible for the phenomenon of *aggregation*, where a crowd of agents is self-organized into one or more large-scale stationary clusters with an observable geometric configuration. Different kernels $\phi(\cdot, \cdot)$ lead to a great variety of different limiting configurations. These are observed in cell biology, with tissue formation (mediated by cell-to-cell recognition and cell adhesion) being the prototypical example [19]; cell aggregation also plays a fundamental role in cellular differentiation [20], proliferation [21, 22] and viability [22, 23]. We mention on passing the important role played by aggregation in cellular viability, for example when it is utilized in biofilms as a survival mechanism for bacterial cells and for cellular adhesion in chemo- and radio-resistance [24–27]. Aggregates of cells also commonly coordinate their movement to collectively migrate; prominent biological processes displaying this behavior are wound healing and cancer invasion [28], as well as chemotaxis and phototaxis [29, 30]. Aggregation is of course not limited to cells; thus, for example, many species of insects (e.g. monarch butterflies overwintering) and animals form complex social structures for a diverse set of evolutionary reasons [31].

A third main feature in emergent dynamics is driven alignment—the steering towards the average heading of neighboring agents. A typical second-order alignment dynamics can be expressed by

$$\dot{\mathbf{p}}_i(t) = -\frac{\tau}{|\mathcal{N}_i(t)|} \sum_{j \in \mathcal{N}_i(t)} \phi(\mathbf{x}_i, \mathbf{x}_j)(\mathbf{p}_i - \mathbf{p}_j). \quad (5)$$

Here, $\tau > 0$ is a fixed scaling parameter and $\mathbf{p}_i$ stands for the velocity of the agent positioned at $\mathbf{x}_i(t)$ [5, 6], $\mathbf{p}_i(t) \mapsto \mathbf{v}_i(t) := \dot{\mathbf{x}}_i(t)$, or its orientation [14, 32, 33], $\mathbf{p}_i(t) \mapsto \boldsymbol{\omega}_i(t) := \mathbf{v}_i(t)/|\mathbf{v}_i(t)| \in \mathbb{S}^{d-1}$. In a typical case of long-range interactions in a crowd of N agents, $|\mathcal{N}_i| = N$, one can adjust to short- and long-range interactions, replacing $|\mathcal{N}_i| \mapsto \sum_j |\phi(\mathbf{x}_i, \mathbf{x}_j)|$ [34]. The alignment encoded in (5) describes environmental averaging of velocities/orientations. Alignment may be either local or global, depending on the heavy-tailed scale of the interaction kernel. Alignment governs the emergent phenomena of flocking or swarming, found in animal populations [35], in which agents attempt to align their heading and/or speed in a large-scale coordinated movement. Schools of fish [36–38], flocks of birds [39–42] and herds of animals [43] are some of the most well-known examples. We mention in passing that the evolutionary roles played by flocking are diverse and species dependent: examples include reproductive efficiency, predation avoidance and route learning in migration [44–46]. Flocking can manifest itself via synchronization, in which pairwise interactions between agents are coordinated in time into large-scale crowd oscillations. Well-known examples include the frequency of flashing of firefly lights [47], the 'chorusing' behavior of some species of crickets [48] and the firing of neurons [49]. Flocking occurs in behavioral contexts as well, with consensus building being an emergent phenomenon in opinion dynamics [50]. It is realized on many different scales, from populations of cells to populations of humans [51].

The full complexity of self-organization observed in biological systems is realized when combining attraction, repulsion and alignment. This was originally advocated in the pioneering work of Reynolds [16] for realistic simulation of boids—birds-like objects. Reynolds' model remains one of the most commonly utilized methods of describing collective motion, with extensions proposed to incorporate the effect of pheromone signaling [52] and obstacle avoidance [53], as well as a motivation for development of particle swarm optimization [54]. The incorporation of social hierarchy via leadership has also been explicitly incorporated into Reynolds' rules for boids using an additional steering force that allows an agent to change the course of the flock based on the agent's position with respect to the flock [55]. We note that although most boid models are presented as discrete velocity update rules, they typically can be

translated to either deterministic or discrete second-order systems (see section 3.2).

A systematic framework for combining attraction, repulsion and alignment mechanisms is offered by anticipation dynamics induced by a radial potential U, and acting at the 'anticipated positions' $\mathbf{x}_i^\tau := \mathbf{x}_i + \tau \mathbf{v}_i$ [56] (here we make the simplification of long-range interactions $|\mathcal{N}_i| = N$)

$$\dot{\mathbf{v}}_i(t) = -\frac{1}{N}\sum_{j=1}^{N} \nabla_i U(|\mathbf{x}_i^\tau - \mathbf{x}_j^\tau|). \tag{6}$$

Expanding at the small 'anticipated time' $t+\tau$, $\tau \ll 1$, one finds

$$\begin{aligned}\dot{\mathbf{v}}_i(t) = &-\frac{1}{N}\sum_j \phi_{ij}(\mathbf{x}_i - \mathbf{x}_j) \\ &+ \frac{\tau}{N}\sum_j \Phi_{ij}(\mathbf{v}_j - \mathbf{v}_i).\end{aligned} \tag{7}$$

Here, attraction and repulsion are dictated by $\phi_{ij} := U'(|\mathbf{x}_i - \mathbf{x}_j|)/|\mathbf{x}_i - \mathbf{x}_j|$, and alignment is dictated by the Hessian $\Phi_{ij} = D^2U(|\mathbf{x}_i - \mathbf{x}_j|)$, with a scalar leading-order term $\psi_{ij} = U''(|\mathbf{x}_i - \mathbf{x}_j|)$. Thus, for example, a standard U-shaped potential-based anticipation dictates three-zone dynamics in three concentric regions, ranging from interior repulsion ($U' < 0$), through intermediate alignment where $U' \sim 0$ and surrounded with exterior attraction ($U' > 0$). Such three-zone dynamics is encountered in many models for flocking and swarming. For example, many species of insects exhibit swarming behavior in which their motion is self-organized into approximately concentric trajectories, known as milling, or vortex formation [57]. This enables the insects to carry out specific tasks in the form of collective intelligence. Examples of swarming include the marching of locust nymphs [58, 59] and lane formation and obstacle avoidance in army ants [33]. Milling is most commonly associated with fish populations during schooling and mating rituals [32, 60]. It also occurs in cell clusters [61, 62], and less frequently in ants during extreme conditions [63].

Finally, we note that although it is not a focus of the present work understanding collective motion for biological crowds has numerous applications in the engineering sciences. Examples include mobile sensing networks and the utilization of cooperative uncrewed aerial vehicles [64–68].

1.2. A new collective model for fingering

Certain forms of emergent behavior can be classified as possessing degrees of social hierarchy, where individual agents conform to distinct roles. As with all emergent behavior, hierarchy can arise across a vast range of scales, from small groups of cells (e.g. in cell migration [69, 70]), to colonies of insects [71], to extraordinarily complex systems in vertebrates [72]. A well-known example occurring in bacterial motion is that of fingering, which serves as a primary motivation for the mathematical model introduced in this work. Fingering is a motility pattern that is often observed in cell cultures and is characterized by cellular populations, which initially undergo essentially random and independent motion, forming structured 'finger-like' protrusions from their initial homogeneous state [73–75]. These protrusions indicate the emergence of social hierarchy via 'leader-type' cells at the leading edge of the protrusions; the remaining cells 'follow' in the paths determined by leading cells, often in very straight lines [75]. Fingering is most closely associated with populations exposed to optical gradients (phototaxis), but is also observed in wound healing, where cellular communication is determined primarily via chemical (chemotaxis) and mechanical signaling [76–79]. The formation of leaders/followers is also observed in other biological systems, such as in trail formation and cooperative transport in groups of ants [33, 80–83] and the marching swarms of locusts as mentioned above [58, 59]. Many biological mechanisms exist by which leader/follower hierarchy emerges, including pheromone signaling [81], slime formation [75] and mechanical pressure [79], although many scientific questions remain [84, 85].

It is the goal of this work to present a minimal mathematical model that describes the emergence of a social hierarchy of leaders and followers via pairwise interactions; for a visualization of typical simulations exhibiting line formation see figure 1. Our proposed model can be understood from a simple phenomenological perspective: rather than metric-based interaction, $\phi_{ij} = \phi(|\mathbf{x}_i - \mathbf{x}_j|)$, we propose projected–based interactions

$$\phi_{ij} = \phi(\chi_{ij}\mathbf{x}_j - \mathbf{x}_i), \quad \chi_{ij} := \frac{\langle \mathbf{x}_i, \mathbf{x}_j\rangle}{|\mathbf{x}_j|^2}, \tag{8}$$

where the agent positioned at $\mathbf{x}_i$ interacts with the *traces* of neighboring agents in the forward-looking cone $\mathbf{x}_j \in \mathcal{N}_i := \{\beta|\mathbf{x}_i|/|\mathbf{x}_j| \leqslant \chi_{ij} \leqslant 1\}$ (figure 5 shows a geometric illustration of the projection). This leads to the spontaneous formation of leaders and followers, defined with respect to their relative positions in a linear aggregate. Observe that the interactions in (8) are not symmetric; further, they are not Galilean invariant. Accordingly, there is a need to shift the fixed origin and trace the dynamics relative to the center of mass, $\mathbf{x}_i \mapsto \mathbf{x}_i - \overline{\mathbf{x}}$.

Such interactions can be readily understood in many of the applications described above, such as the sensing of pheromone trails left by neighboring ants and slime model deposits in bacterial cultures. Although inspired by fingering in phototaxis and chemotaxis, the model assumes no external forcing, so that the emergence of lines is intrinsic to the interactions of the agents alone. Furthermore, the

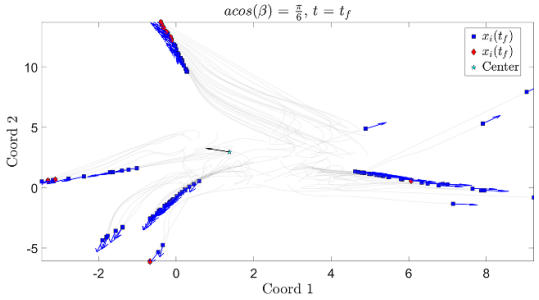

Figure 1. Trajectory plot of the second-order system described in section 3.2 with the initial configuration shown in figure 2. The coloring of the agents is described in the caption of figure 2, and the gray trailing lines indicate the path of an agent's trajectory. Note that the agents furthest away may not become 'leaders'.

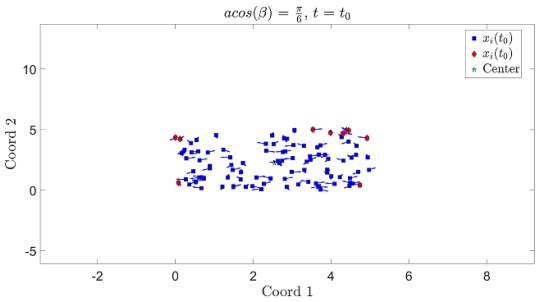

Figure 2. Initial configuration of positions/velocities of a second-order system as described in section 3.2. We simulate $N = 100$ agents (blue squares), with 10 agents (red diamonds) chosen at the initial time as the furthest from the center of mass (cyan star) at $t_0 = 0$.

model is sufficiently generic to describe a wide variety of phenomena, including spatial positions and velocity, but also emotions, frequencies, headings, opinions, etc as described previously.

The remainder of the paper is organized as follows. We provide a brief discussion of the mathematical models of collective motion and chemotaxis/phototaxis in section 2. In section 3, we provide a detailed description of the modeling framework, with details of the first- and second-order systems provided in sections 3.1 and 3.2, respectively. The formation of lines in first-order systems is summarized in theorem 1 in section 4; Numerical results are provided in section 5, and concluding remarks are provided in section 6.

2. Alignment models of collective motion and social hierarchy

In this section we restrict our attention to alignment dynamics, suppressing the additional roles of attraction and repulsion. We begin with a brief overview of two alignment models: we refer to [17, 18] for a thorough discussion on the biological phenomena and to [4] for a recent mathematically rigorous discussion of alignment models. The first alignment model originates from the 1995 work of Vicsek *et al* [14], in which self-propelled particle systems go through local averaging of velocity orientations. Indeed, many physical and biological systems utilize one form or another of environmental averaging [86–90]. A second velocity alignment model was introduced in 2007 by Cucker and Smale [5, 6]. The model presented in this manuscript is directly inspired by the Cucker–Smale (CS) model, so we describe it in detail here. The system consists of N identical interacting agents, each identified by its position $\mathbf{x}_i$ and velocity $\mathbf{v}_i$ in $\mathbb{R}^d$, for $i = 1, 2, \ldots, N$. Their dynamics is governed by

$$\begin{aligned} \dot{\mathbf{x}}_i(t) &= \mathbf{v}_i \\ \dot{\mathbf{v}}_i(t) &= \frac{\tau}{N}\sum_{j=1}^{N} \phi_{ij}(t)(\mathbf{v}_j(t) - \mathbf{v}_i(t)), \end{aligned} \tag{9}$$

with pairwise interactions driven by $\phi_{ij}(t) = \phi(\mathbf{x}_i(t), \mathbf{x}_j(t))$. The scalar *communication kernel*, ϕ, quantifies the dynamic influence of agent j on agent i. In the original CS model, the authors advocate a class of long-range decreasing metric kernels

$$\phi_{ij} = \phi(|\mathbf{x}_i - \mathbf{x}_j|), \quad \phi(r) = \frac{K}{(\alpha^2 + r^2)^\beta}, \tag{10}$$

with constants $K, \beta > 0$. We previously discussed other classes of singular kernels that emphasize nearby agents over those farther away [11–13, 91, 92], $\phi(r) = r^{-\beta}$, and the class of short-range kernels, $\phi(r) = \mathbb{1}_{r \leqslant r_0}$. Metric kernels reflect, by definition, symmetric interactions, $\phi_{ij} = \phi_{ji}$, and we notice the tacit assumption that communication decays with distance. Motivated by the original CS model, the general framework of alignment based on pairwise interactions has inspired considerable work, including the hydrodynamic description of its large crowd limit [2, 9, 93–96], incorporation of collision avoidance [97], steering [98] and stochasticity [99]. The large-time behavior of CS alignment dynamics (9) should lead the crowd to aggregate into a finite-size cluster, $\max |\mathbf{x}_i(t) - \mathbf{x}_j(t)| \leqslant D$, which in turn leads to flocking $|\mathbf{v}_i(t) - \mathbf{v}_j(t)| \overset{t\to\infty}{\longrightarrow} 0$. However, left without attraction/repulsion, dynamics driven solely by alignment does not support the emergence of any preferred spatial configuration.

As mentioned in section 1, the goal of this work is to provide a minimal mathematical model that exhibits the emergence of a simple form of social hierarchy through pairwise interactions. The model is a direct analog of CS alignment and is inspired by the biological phenomenon of fingering in chemotaxis and photoaxis. It is advocated as a simple alignment mechanism by which a priori identical agents

evolve to form fingering structures with internal hierarchy. It should be emphasized that here, no attempt was made to model the external environment, which is of course necessary to accurately describe an externally signaled process such as phototaxis/chemotaxis; instead, we limit ourselves to cellular inter-communication mechanisms which, we claim, are an essential part of the more complicated processes. In this sense, this work is complimentary to theoretical and experimental work studying social hierarchy as well as chemotaxis/phototaxis. For example, many works formulate interacting agent systems similar to the Vicsek model [100], which may include an internal excitation variable to model phototaxis both deterministically [101] and stochastically [102–104]. Slime deposition [105] is also a common mechanism used to describe fingering, with agent-based [30, 106] and continuum partial differential equations [75] being proposed. Similar approaches exist in describing chemotaxis, including modeling fingering as a free boundary value problem [107], and extensions to the classical chemotaxis equations introduced by Keller and Segel [108–110]. Hierarchy and leadership have been investigated in the CS model [111] as well as in network graphs with switching topologies [112]. Leadership arising via external signaling was introduced and analyzed in [113], moreover leadership in cells due to feedback in speed and curvature can be formed [114–116], which we note may be particularly relevant for phototaxis and chemotaxis.

3. Mathematical models of line alignment

Motivated by the discussion in section 1, we propose both first- and second-order models that describe the emergence of hierarchical structure in interacting agent systems for active particles, which we term generally 'line alignment models'. For both systems, we consider a total of N interacting agents. Each agent is assigned a position $\mathbf{x}_i \in \mathbb{R}^d$, and, in the case of second-order models, agents are assigned an additional velocity $\mathbf{v}_i \in \mathbb{R}^d$. We utilize the projected position $\chi_{ij}\mathbf{x}_j$ as a way to realize the tendency of agents 'to look ahead'. In order to avoid the discussion of absolute origin, we also use the center of mass position of the whole system as the reference. We believe that this assumption is physically reasonable, as groups of bacteria/cells/animals should not utilize a global coordinate system with specified fixed origin but rather measure positions with respect to their local environment, for example the center of mass of their flock, school or other social structural unit. Coordinate systems in local environments may be species dependent; for example, bacteria undergoing phototaxis may measure their position relative to a dominant light source [117] while humans at a concert may measure their positions with respect to the main stage. In an isotropic environment, a 'natural' coordinate system is the center of mass reference frame. That is, we assume that the interacting agents measure their positions relative to the agent-system itself. For example, we consider the relative positions $\widetilde{\mathbf{x}}_i$ and $\widetilde{\mathbf{x}}_j$ defined with respect to the center of mass $\bar{\mathbf{x}}$ of the system

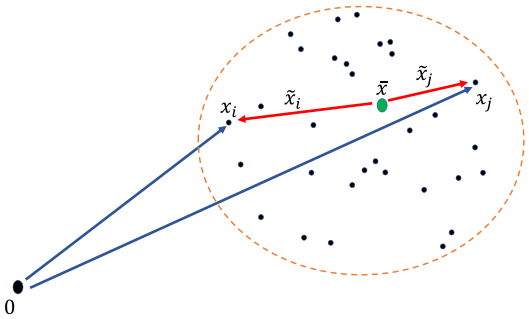

Figure 3. Absolute versus relative position coordinates for agents i and j. Agents are indicated in black, the center of mass of the system $\bar{\mathbf{x}}$ is green, absolute positions are blue and relative positions (with respect to the center of mass) are red. Position vectors are indicated for two representative agents only. Note that the center of mass is calculated for the entire N-agent system (see equation (11)).

$$\widetilde{\mathbf{x}}_i := \mathbf{x}_i - \bar{\mathbf{x}}, \quad \bar{\mathbf{x}}(t) := \frac{1}{N}\sum_{i=1}^{N}\mathbf{x}_i(t). \tag{11}$$

Here $\mathbf{x}_i$ and $\mathbf{x}_j$ denote the positions of the agents with respect to an arbitrary origin $0 \in \mathbb{R}^d$. This is visualized in figure 3. We note that when interactions occur through symmetric differences of positions, as in the CS and Vicsek models, absolute versus relative positions result in identical dynamical systems so that the distinction is irrelevant. However, when considering non-symmetric interactions that arise via projected distances, as in (8), the resulting systems possess distinct vector fields. Of course, certain species may indeed have global coordinate systems, such as in the mass migration of some species of birds [118].

3.1. First-order model

We begin by introducing a first-order model, which governs the positions of N interacting agents (cells, birds, humans, etc). Each agent is described by its time-dependent position $\mathbf{x}_i(t) \in \mathbb{R}^d$. Their dynamics is governed by pairwise interactions

$$\dot{\mathbf{x}}_i(t) = \frac{1}{|\mathcal{N}_i(t)|}\sum_{j\in\mathcal{N}_i(t)}\phi_{ij}(\chi_{ij}\widetilde{\mathbf{x}}_j - \widetilde{\mathbf{x}}_i). \tag{12}$$

Here $\phi_{ij}(t)$ quantifies the interactions, depending on the projected difference

$$\phi_{ij} := \phi(|\chi_{ij}\widetilde{\mathbf{x}}_j - \widetilde{\mathbf{x}}_i|), \quad \chi_{ij} := \frac{\langle\widetilde{\mathbf{x}}_i, \widetilde{\mathbf{x}}_j\rangle}{|\widetilde{\mathbf{x}}_j|^2}. \tag{13}$$

Note that in the case that $|\widetilde{\mathbf{x}}_j| = 0$ (i.e. agent j is located at the center of mass of the system), the projection χ_{ij} is defined as zero. The neighborhood of the agent positioned at $\mathbf{x}_i$ is formed via a *forward cone*, which models the asymmetric phenomenon of 'looking ahead'

$$\mathcal{N}_i := \{j \,|\, \beta|\widetilde{\mathbf{x}}_i||\widetilde{\mathbf{x}}_j| \leqslant \langle \widetilde{\mathbf{x}}_i, \widetilde{\mathbf{x}}_j\rangle \leqslant |\widetilde{\mathbf{x}}_j|^2\}, \tag{14}$$

where $0 < \beta \leqslant 1$ is a fixed constant that determines the angular size of the forward cones[4]. As before, $\phi(\cdot)$ is a communication kernel that quantifies the dynamic influence of the traced agent j on the agent positioned at $\mathbf{x}_i$. In this work, we limit ourselves to metric communication kernels.

To model line alignment, we specify both the pairwise interaction of agents at distance $r_{ij} = |\chi_{ij}\mathbf{x}_j - \mathbf{x}_i|$ and the spatial neighborhoods defining which agents influence the dynamics of one another. The spatial neighborhoods are necessarily non-symmetric, but rather 'forward-facing'; for example, if the agent positioned at $\mathbf{x}_i$ is positioned ahead and 'in view' of the agent positioned at $\mathbf{x}_j$, then agent j should be influenced by agent i, but not vice versa. The notions of positioned ahead and in view of are quantified via $\mathcal{N}_i$, the neighborhood of agent i, i.e. the set of agents that influence the dynamics of agent i.

Note that we use relative coordinates $\widetilde{\mathbf{x}}_i$ and $\widetilde{\mathbf{x}}_j$ to determine the forward cone, based at the corresponding center of mass $\bar{\mathbf{x}}$. Each cone is defined via a central angle of $2\cos^{-1}(\beta)$ radians, which is symmetric about the $\widetilde{\mathbf{x}}_i$ direction; this is the left-hand inequality in (14). The right-hand inequality ensures that agents are only influenced by other agents in front of them in relative position space, so that the cone is indeed forward-facing. The latter can be understood by noting that the right-hand inequality in (14) restricts the length of the projection of $\widetilde{\mathbf{x}}_i$ along $\widetilde{\mathbf{x}}_j$, i.e. $|\widetilde{\mathbf{x}}_i|\cos(\phi) \leqslant |\widetilde{\mathbf{x}}_j|$ where ϕ is the angle between $\widetilde{\mathbf{x}}_i$ and $\widetilde{\mathbf{x}}_j$, so that we require $\widetilde{\mathbf{x}}_j$ to be ahead of $\widetilde{\mathbf{x}}_i$ in relation to $\bar{\mathbf{x}}$. Since all positions $\widetilde{\mathbf{x}}_i$ are time-varying, each $\mathcal{N}_i$ changes in time t; a static visualization of the conic spatial region is provided in figure 4. Geometrically, the influence of agent j on its dynamics, agent i measures its difference in projected position relative to agent j. Thus, the form of (12) tends to align agents along lines, as the pairwise interactions 'aim' to reduce the orthogonal distance between agents i and j. As ϕ is tacitly assumed to be decreasing, agents are more influenced by their nearer neighbors inside the forward-looking cone, i.e. by those that are more aligned with their current direction. This is visualized in figure 5. To completely specify the dynamics, a set of initial conditions $\{\mathbf{x}_i(0)\}_{i=1}^N$ must also be prescribed. Details on the initial conditions and other parameters investigated are provided in section 5.1.

[4] For simplicity, we assume the opening of forward-looking cones to be the same for all agents.

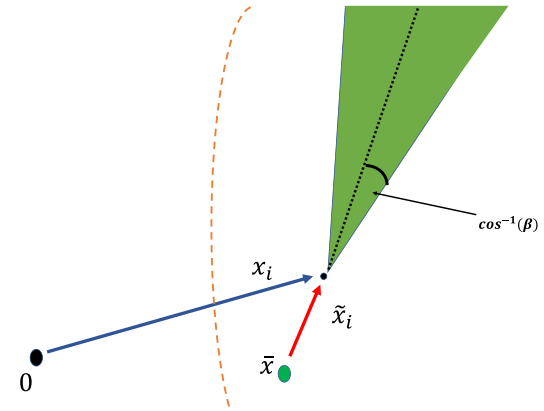

Figure 4. Forward cone defining a neighborhood $\mathcal{N}_i$ for agent i in system (12). The green forward conic region indicates the spatial region defining $\mathcal{N}_i$ in (14). Note that all positions depend on time t, so that the conic region moves with the agents in time.

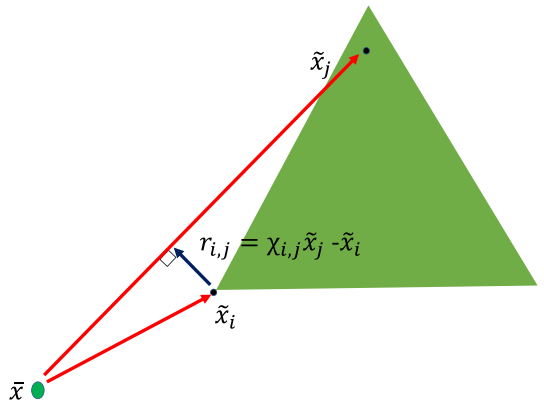

Figure 5. Difference vector $\mathbf{r}_{ij}$ measuring the difference between $\widetilde{\mathbf{x}}_i$ and its projection along $\widetilde{\mathbf{x}}_j$. Vector $\mathbf{r}_{ij}$ measures how aligned agent i is with respect to agent j. Line alignment implies that agent i acts to reduce $\mathbf{r}_{ij}$ for all agents j in its forward cone.

3.2. Second-order model

We now turn to discuss the second-order model, analogous to the first-order model detailed in section 3.1, but in which pairwise interactions influence the acceleration of the agents; this is in contrast to (12), where agents directly regulate velocity. This framework is more closely related to a classical mechanics perspective, where the interaction terms are precisely interaction *forces*. The state-space is represented by the position and velocity vectors of the N agents, i.e. $\{\mathbf{x}_i, \mathbf{v}_i\}_{i=1}^N$, where the second-order dynamics reads

$$\begin{aligned}\dot{\mathbf{x}}_i(t) &= \mathbf{v}_i(t)\\ \dot{\mathbf{v}}_i(t) &= \frac{1}{|\mathcal{N}_i(t)|}\sum_{j\in\mathcal{N}_i(t)}\Big(\phi(|\mathbf{r}_{ij}(t)|)\mathbf{r}_{ij}(t)\\ &\quad + \psi(|\mathbf{r}_{ij}(t)|)(\mathbf{v}_j(t) - \mathbf{v}_i(t))\Big)\end{aligned} \tag{15}$$

Here $\mathbf{r}_{ij} := \chi_{ij}\widetilde{\mathbf{x}}_j - \widetilde{\mathbf{x}}_i$ denotes the orthogonal component of $\widetilde{\mathbf{x}}_i$ projected in the direction of $\widetilde{\mathbf{x}}_j$, so that agents interact via relative projected directions as discussed in section 3.1 (see equation (13)), and hence act to align 'along lines'. The functions ϕ and ψ characterize the strength of the interactions; both depend on the projected distances, $r_{ij} = |\mathbf{r}_{ij}|$, between agents currently positioned at $\widetilde{\mathbf{x}}_i$ and the agent currently positioned at $\widetilde{\mathbf{x}}_j$, which is traced to its backward position $\chi_{ij}\widetilde{\mathbf{x}}_j$. Interactions are again local, and the net effect on the dynamics of agent i is the superposition of the interaction forces from all 'forward-looking' neighboring agents $j \in \mathcal{N}_i$.

The pairwise interactions are determined by the two function ϕ and ψ. We first observe that the force governed by ϕ is identical to that of the first-order attraction/repulsion in (4). The second term, dictated by interaction kernel ψ, is an extension of the CS velocity alignment force [5, 6]. The velocity alignment in our second-order model ensures that, in equilibrium, the emergent 'finger-like' lines lead to flocking, $|\mathbf{v}_i(t) - \mathbf{v}_j(t)| \overset{t\to\infty}{\longrightarrow} 0$. Indeed, the line formation will remain stable only when all the agents are moving with the same velocity; otherwise the lines formed will not be stable.

4. From alignment to the emergence of lines

The key feature of the first- and second-order models, (12) and (15), respectively, is the emergence of geometric structure for the trails along which the crowd is aligned. Specifically, we observe the large-time formation of curves turning into straight lines (see the numerical simulations reported in section 5). A detailed analysis of this phenomenon is beyond the scope of this paper and will be provided in future work. Here we quote a prototypical result. We consider the first-order line alignment model

$$\begin{aligned} \dot{\mathbf{x}}_i(t) &= \frac{\tau}{\sigma_i}\sum_{j\in\mathcal{N}_i(t)} \phi_{ij}\big(\chi_{ij}\mathbf{x}_j(t) - \mathbf{x}_i(t)\big), \\ \chi_{ij} &= \frac{\langle \mathbf{x}_i, \mathbf{x}_j\rangle}{|\mathbf{x}_j|^2}, \quad \sigma_i := \sum_{j\in\mathcal{N}_i}\phi_{ij}. \end{aligned} \tag{16}$$

To simplify our discussion, we set the dynamics relative to a fixed origin, so that $\widetilde{\mathbf{x}}_i \mapsto \mathbf{x}_i$. The specifics of the projected communication, given by $\phi_{ij} = \phi(\chi_{ij}\mathbf{x}_j - \mathbf{x}_i)$, are not essential; indeed, it is remarkable that our results apply to a wide variety of communication protocols independent of symmetry or occupying a global stencil. Here, we use an adaptive normalization of the communication protocol as in [34], replacing $N_i \mapsto \sigma_i$, so that $\frac{1}{\sigma_i}\sum_{j\in\mathcal{N}_i}\phi_{ij} = 1$ (so that the dynamics does not involve 'counting' the number of agents).

Theorem 1. *Consider the line alignment model (16), dictated by a decreasing kernel $\phi(r)$, which acts inside the forward-looking cones*

$$\mathcal{N}_i := \{j \,|\, \beta|\mathbf{x}_i||\mathbf{x}_j| \leqslant \langle \mathbf{x}_i \mathbf{x}_j\rangle \leqslant |\mathbf{x}_j|^2\}, \quad \beta > 0.$$

Then, there exist constants C_0, depending on the initial configuration, and C_ϕ, depending on ϕ, such that the following holds:

$$\sum_i \sum_{j\in\mathcal{N}_i}\Big(|\mathbf{x}_i(t)|^2\cdot|\mathbf{x}_j(t)|^2 - |\langle \mathbf{x}_i(t), \mathbf{x}_j(t)\rangle|^2\Big) \leqslant C_0 e^{-C_\phi \beta^2 t}.$$

Theorem 1 precisely quantifies the emergence phenomenon in the first-order model (12). Namely, the crowd forms one or more distinct straight trails, led by an agent $\mathbf{x}_i$ and followed by its neighbors $\{\mathbf{x}_j,\ j\in\mathcal{N}_i\}$ so that $|\mathbf{x}_i|\cdot|\mathbf{x}_j| - \langle \mathbf{x}_i, \mathbf{x}_j\rangle \overset{t\to\infty}{\longrightarrow} 0$. The remarkable aspect of the line dynamics, reflected in theorem 1, is that the 'kinetic energy' $\sum_i\sum_{j\in\mathcal{N}_i}|\mathbf{x}_i(t)|^2\cdot|\mathbf{x}_j(t)|^2$ is easily shown to be decreasing in time. However, the 'potential energy' $\sum_i\sum_{j\in\mathcal{N}_i}|\langle \mathbf{x}_i(t), \mathbf{x}_j(t)\rangle|^2$ does not exhibit a time-monotone behavior and may change with the configuration. It is their difference that is decreasing in time, reflecting the emergent behavior. To our knowledge, this represents the first large-time, large-crowd emergence dynamics based on *local* interactions (the neighborhoods $\mathcal{N}_i$s).

5. Numerical results

In this section, we numerically investigate the models of social hierarchy presented in section 3. Specifically, we demonstrate the emergence of lines in both the first- and second-order models, and study the effect of model parameters, including the number of agents and type of interaction kernel, on the resulting dynamics. We also show that the formation of a leader agent is indeed emergent and cannot be easily extrapolated via initial conditions alone.

5.1. First-order model line formation

We begin by simulating the first-order line alignment model (12) with the parameters appearing in table 1. We are thus simulating $N = 100$ agents over a period of 50 time units in two spatial dimensions. Here μ_0 denotes a probability distribution utilized for generating the initial positions, with $\mathcal{U}([0,5]^2)$ representing the uniform distribution over $[0,5]^2$. Thus, we assume that the agents are initially uniformly distributed over a square region in the plane. A fixed realization of initial positions of agents is used for all simulations in this subsection, and is provided in figure 6. In this subsection, we assume a topological interaction kernel as discussed in section 1:

$$\phi(r) = \mathbb{1}_{r\leqslant 1}(r) \quad \text{or} \tag{17}$$

Table 1. Parameters utilized to simulate the first-order model as discussed in section 5.1.

μ_0	d	N	t_0	t_f
$\mathcal{U}([0,5]^2)$	2	100	0	50

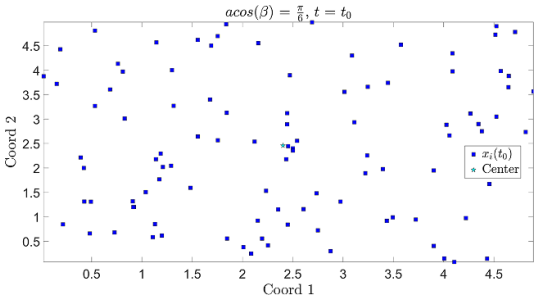

Figure 6. Initial configuration of the positions of $N = 100$ agents for a first-order system with parameters as in table 1.

$$\phi(r) = \frac{1}{(1+r^2)^{0.25}}, \tag{18}$$

where r denotes the projected difference between agents with respect to an agent's forward cone (see equation (13)). Recall that $\mathbb{1}_{r\leqslant 1}$ denotes the indicator function on the set $[0,1]$, so that all agents with a projected distance less than one unit inside the forward cone have an equal influence on the dynamics of the agent. All simulations, in this and other sections, are integrated using MATLAB's built-in adaptive integrator ode 23 for handling possible stiffness of the system.

We begin by demonstrating that the proposed first-order model asymptotically exhibits line formation. Consider figure 7, which assumes a forward cone with central angle $\pi/3$ and an interaction kernel given by (17). Blue squares in the figure represent agent positions $\mathbf{x}_i(t)$ and the cyan star represents the center of mass position of the system, i.e. $\bar{\mathbf{x}}_i(t)$. Recall that the center of mass is not stationary, and that all agents measure relative coordinates with respect to $\bar{\mathbf{x}}_i(t)$. In this figure, we clearly observe the formation of spatial lines that originate from the center of mass of the system. This hierarchical structure emerges from the initial uniform distribution of positions in figure 6, and hence can be thought of as a form of emergence of social hierarchy. Note that the 'leaders' here correspond to the agents farthest from the center of mass of the system. The dynamics thus represent a rudimentary form of finger morphology as discussed in section 1.2, which occurs through purely inter-agent interactions, with no reliance on external forces. It may appear that the leaders form from those agents initially farthest from the center of mass of the system, but this is not necessarily true (see section 5.6 for

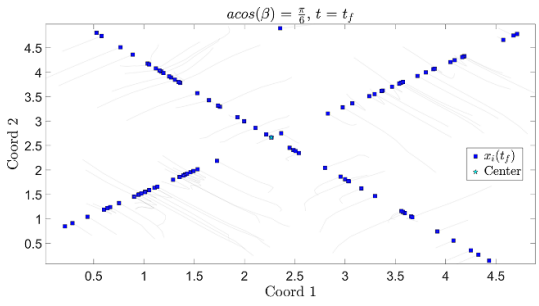

Figure 7. Trajectory plot for the first-order system with parameters taken from table 1 with $\beta = \frac{\pi}{6}$ and $\phi = \mathbb{1}_{r\leqslant 1}$. The initial configuration of positions is shown figure 6. We clearly observe the formation of lines.

details regarding the second-order model). We also emphasize that the system has reached equilibrium, as simulating later in time (not shown) produces the same spatial pattern observed in figure 7.

5.2. Variation of dynamics as a function of forward cone size

We investigate the dynamics of line formation as a function of the size of the forward cone. Specifically, we are interested in understanding the effect of the angular size of the cone, defined by β (see figure 4), on the dynamics of line formation. Questions of specific interest are the number and density of lines formed, which thus correspond to the number of emergent leaders (equivalently, the number of 'fingers' formed). Intuitively, we expect that the number of lines formed should increase as the size of the forward cone decreases, as each agent acts with a higher degree of locality. For a demonstration see figure 8, which utilizes the same initial conditions and parameters as in figure 7, with the exception that a central angle corresponding to π defines the forward cone (note that in this case it is really a forward *plane* and not a cone). We observe a similar pattern of lines compared to the smaller, and hence more local, forward cone, but with a significantly higher degree of clustering to points, so that the asymptotic behavior is more similar to *points* as opposed to lines. The mechanism that produces this behavior is due to a combination of two factors: (1) the dynamics are first-order, and hence tend to exhibit aggregation, and (2) the interaction kernel (17) assumes a uniformity of influence with respect to all neighboring agents. To see the resulting pattern formation and the effect of varying β for the CS interaction kernel (18), see section 5.4.

5.3. Variation of dynamics as a function of initial conditions

In the previous section, we studied line formation for a fixed set of initial conditions. Also of interest is the role of initial conditions on the distribution of

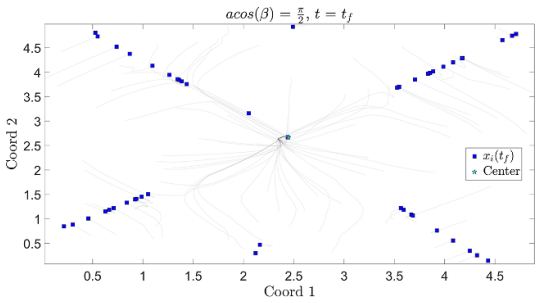

Figure 8. Trajectory plot for the first-order system with parameters taken from table 1 with $\beta = \frac{\pi}{2}$ and $\phi = \mathbb{1}_{r\leqslant 1}$. The initial configuration of positions is shown in figure 6. We clearly observe the formation of lines, with significant clustering about the center of mass (compare with figure 7).

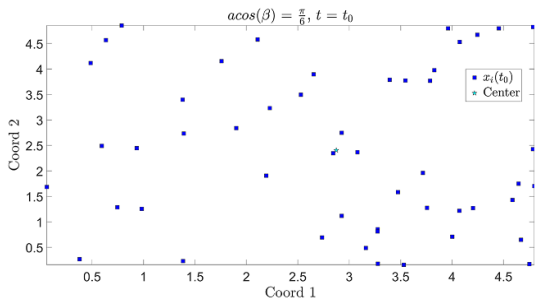

Figure 9. Initial configuration of positions for a first-order system with the parameters taken from table 1, except for a smaller number of agents ($N = 50$).

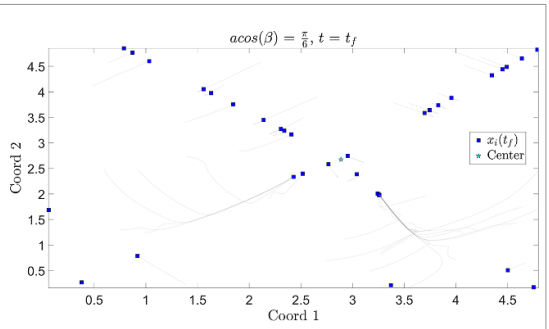

Figure 10. Trajectory plot for the first-order system with parameters taken from table 1 with $\beta = \frac{\pi}{6}$ and $\phi = \mathbb{1}_{r\leqslant 1}$. The initial configuration of positions is shown in figure 9.

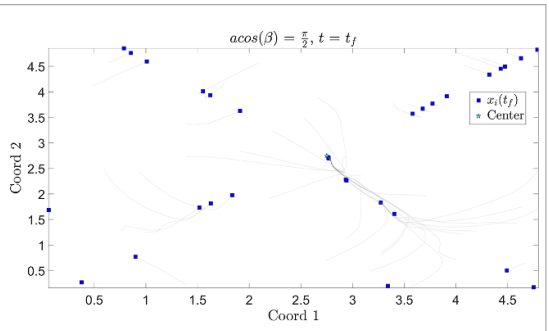

Figure 11. Trajectory plot for the first-order system with parameters taken from table 1 with $\beta = \frac{\pi}{2}$ and $\phi = \mathbb{1}_{r\leqslant 1}$. The initial configuration of positions is shown in figure 9.

lines. More precisely: is the resulting pattern robust or highly sensitive to the agents' initial positions? Numerical simulations (not provided) suggest that the final configuration of lines (both the number of lines and their orientations) is highly dependent on the initial conditions; resampling μ_0 generally results in a different equilibrium distribution. We note that this is not surprising, and it is a common feature of models describing collective motion. Similarly, we investigate how the behavior changes as a function of the number of agents (N in table 1). This is a natural scientific question, as line formation occurs across a variety of scales; for example, the number of ants composing a trail may be of the order of 100, while the number of bacteria generating finger morphology in phototaxis may be of the order of 1000. Furthermore, such questions are of mathematical interest, as they may provide insight into corresponding coarse-grained macroscopic models, such as mean-field Vlasov-type equations and the corresponding hydrodynamic descriptions. We thus investigate to what degree the social hierarchy model proposed in this work is dependent on the number of agents in the system. As an example, we repeat simulations appearing in figures 7 and 8 with fewer agents ($N = 50$ versus $N = 100$ previously; new initial conditions are provided in figure 9); the corresponding results can be found in figures 10 and 11. Similar qualitative dynamics are apparent for the smaller system, but in general we see that the distributions of lines is quite different, even for the corresponding forward cones.

5.4. Effect of interaction function on pattern formation

In the previous sections we assumed a topological interaction kernel given by (17), which weights all neighboring agents equally in a forward cone with limited support. We here instead use a global interaction function, i.e. $\phi = \frac{1}{(1+r^2)^{0.25}}$, to demonstrate the effect of the interaction function on line formation for two different β values. As discussed in section 5.2, we expect a global kernel to exhibit a more pronounced response to the size of the forward cone with respect to angle β. Results of simulations are provided in figures 12 and 13. Compared with the locally supported ϕ (figures 7 and 8), the final distribution of lines in this system shows considerable variation: two lines for $\beta = \pi/6$ become one for $\beta = \pi/2$. Note that the initial configuration of positions is the same as that shown in figure 6.

5.5. Second-order model simulation results

We next simulate the second-order model (15) to demonstrate the dynamics of line formation in a system where interactions affect acceleration; simulation details are provided in table 2. Recall from section 3.2 that we must specify two interaction kernels: ϕ, which

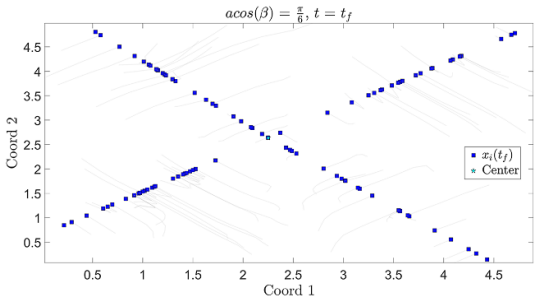

Figure 12. Trajectory plot for the first-order system with parameters taken from table 1 with $\beta = \frac{\pi}{6}$ and $\phi = \frac{1}{(1+r^2)^{0.25}}$. The initial configuration of positions is shown in figure 6.

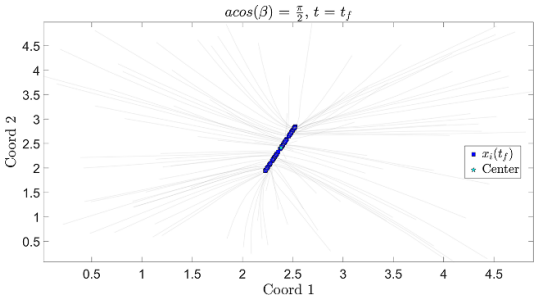

Figure 13. Trajectory plot for the first-order system with parameters taken from table 1 with $\beta = \frac{\pi}{2}$ and $\phi = \frac{1}{(1+r^2)^{0.25}}$. The initial configuration of positions is shown in figure 6.

Table 2. Parameters utilized to simulate the second-order model as discussed in section 5.5.

$\mu_0^{\mathbf{x}}$	$\mu_0^{\mathbf{v}}$	d	N	t_0	t_f	ϕ	ψ
$[0,5]^2$	$\mathbb{B}^2$	2	100	0	10	$\mathbb{1}_{r\leqslant 1}$	$\frac{1}{(1+r^2)^{1/2}}$

governs the inter-agent interaction force of line alignment, and ψ, which accounts for velocity alignment and hence stabilization. Note that ϕ is completely analogous to the first-order model except that it more directly corresponds to a classical Newtonian force law as the system is second-order. We assume the same function dependence (17) for ϕ and assume the classical CS interaction kernel for ψ

$$\psi(r) = \frac{1}{(1+r^2)^{1/2}}. \tag{19}$$

Here $\mathbb{B}^2$ is the two-dimensional unit ball centered at the origin. We simulate the models for different values of β to investigate the effect of the various neighborhood sizes, as in section 5.2 for the first-order model. All tests use the same initial conditions, with the initial position $\mathbf{x}_i(t_0)$ being an independent and identically distributed (iid) sample from $\mu_0^{\mathbf{x}}$ and the initial velocity being an iid sample from $\mu_0^{\mathbf{v}}$. Figure 14 provides the realization of the initial

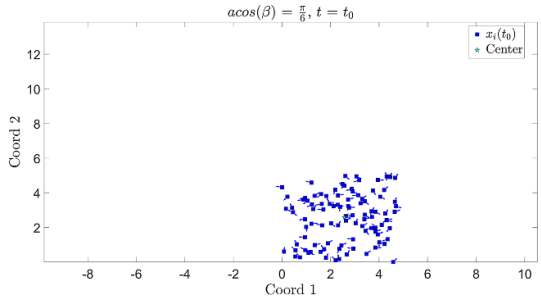

Figure 14. Initial configuration of positions and velocities for a second-order system of $N = 100$ agents with the parameters taken from table 2.

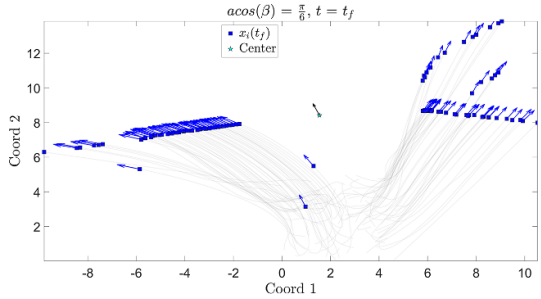

Figure 15. Trajectory plot for the second-order system with parameters taken from table 2 with $\beta = \frac{\pi}{6}$. The initial configuration of positions/velocities is shown in figure 14.

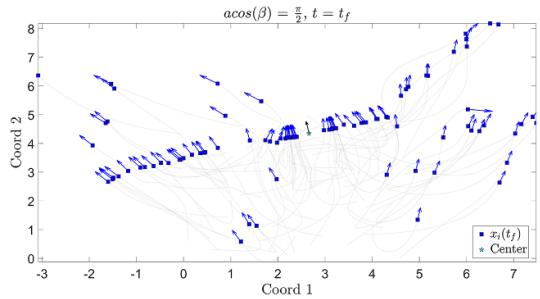

Figure 16. Trajectory plot for the second-order system with parameters taken from table 2 with $\beta = \frac{\pi}{2}$. The initial configuration of positions/velocities is shown in figure 14.

configuration of positions/velocities for all the tests of different β values investigated in this work. The blue dots in the figures represent the position (i.e. $\mathbf{x}_i(t)$) of the agents, with the yellow arrow representing the velocity (i.e. $\mathbf{v}_i(t)$), whereas the cyan dot represents the center of mass position and $\bar{\mathbf{x}}_i(t)$ with the yellow arrow represents the center of mass velocity $\bar{\mathbf{v}}_i(t)$. Results are provided in figures 15–19, where we have again considered variation in forward cone size (β) and the number of agents ($N = 100$ versus $N = 50$). The results are qualitatively similar to the first-order system, although the second-order system exhibits a much richer class of dynamics, as the system does not approach equilibrium configurations

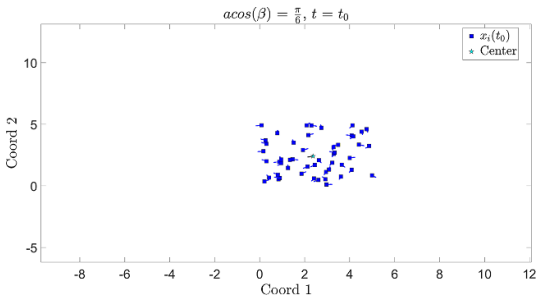

Figure 17. Initial configuration of positions for a second-order system with the parameters taken from table 2 for two different β values and $N = 50$.

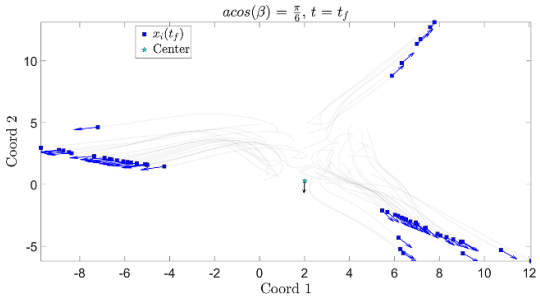

Figure 18. Trajectory plot for the second-order system with parameters taken from table 2 with $\beta = \frac{\pi}{6}$. The initial configuration of positions/velocities is shown in figure 17.

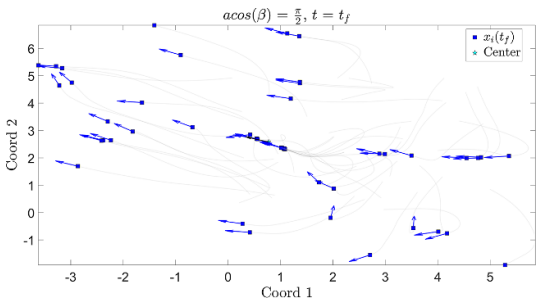

Figure 19. Trajectory plot for the second-order system with parameters taken from table 2 with $\beta = \frac{\pi}{2}$. The initial configuration of positions/velocities is shown in figure 17.

(this is because inter-agent forces act on accelerations and not velocities, i.e. the system is not dissipative). Note that local groups of agents initially form curved lines of hierarchy ('leaders–followers') which eventually straighten due to the projected interaction kernel (figure 1). It thus appears that the competition between line formation (induced by ϕ_1) and flocking (induced by ϕ_2) has made the emergent pattern more interesting. As shown in three of the four examples of different β (with larger β), the system as a whole can produce different flocking velocities, yet social hierarchy (in this case, lines) can emerge from the initially chaotic configuration.

5.6. Initial conditions are not simple predictors of leader emergence

We note that the emergence of leaders is not a simple function of the initial distance from the initial center of mass; thus hierarchy is indeed emergent from the proposed inter-agent dynamics. Consider figure 1, which shows a number of flocking lines ('fingers') emerging from an initially random distribution of positions and velocities (figure 14). In figure 1, we have colored red the 10 initial agents farthest from the initial center of mass. Note that some agents that were initially farthest from the center of mass become followers; for example, on the right-hand side there is a line of agents with an initially distant agent (red) that becomes a 'follower'. Similarly, we see that some agents that were initially near the center of mass become 'leaders' of groups of agents. Hence, we see that the model does indeed exhibit emergence of social hierarchy.

6. Discussion and conclusions

In this work, we have presented two collective dynamic models, namely a first-order and a second-order system, where the emergence of social hierarchy, or 'line formation', is induced from the 'look-ahead' tendency of agents. These two models are minimal in a sense that the 'look-ahead' tendency is implemented using a projected distance together with a forward-cone neighborhood. These models show promising features of natural emergence of geometric structures for various different kinds of initial configurations. More complicated patterns can be induced by using different types of communication kernels (ϕ or ψ). We have presented numerous numerical simulations and are currently developing a mathematical theory to rigorously understand properties of the emergence of line formation in such models.

Data availability statement

All data that support the findings of this study are included within the article (and any supplementary files).

Acknowledgments

Research of ET was supported in part by ONR Grant N00014-2112773. Research of MZ was supported in part by NSF Grant CCF-AF-2225507.

ORCID iD

Eitan Tadmor https://orcid.org/0000-0001-7424-6327

References

[1] Parrish J K and Hamner W M 1997 *Animal Groups in Three Dimensions: How Species Aggregate* (Cambridge: Cambridge University Press)

[2] Motsch S and Tadmor E 2014 Heterophilious dynamics enhances consensus *SIAM Rev.* **56** 577–621

[3] Shvydkoy R *et al* 2021 *Dynamics and Analysis of Alignment Models of Collective Behavior* (Berlin: Springer)

[4] Tadmor E 2021 On the mathematics of swarming: emergent behavior in alignment dynamics *Not. AMS* **68** 493–503

[5] Cucker F and Smale S 2007 Emergent behavior in flocks *IEEE Trans. Autom. Control* **52** 852–62

[6] Cucker F and Smale S 2007 On the mathematics of emergence *Japan. J. Math.* **2** 197–227

[7] Ballerini M *et al* 2008 Interaction ruling animal collective behavior depends on topological rather than metric distance: evidence from a field study *Proc. Natl Acad. Sci. USA* **105** 1232–7

[8] Shvydkoy R and Tadmor E 2020 Topologically based fractional diffusion and emergent dynamics with short-range interactions *SIAM J. Math. Anal.* **52** 5792–839

[9] Ha S-Y and Tadmor E 2008 From particle to kinetic and hydrodynamic descriptions of flocking *Kinetic Relat. Models* **1** 415–35

[10] Ha S-Y and Liu J-G 2009 A simple proof of the Cucker–Smale flocking dynamics and mean-field limit *Commun. Math. Sci.* **7** 297–325

[11] Peszek J 2015 Discrete Cucker–Smale flocking model with a weakly singular weight *SIAM J. Math. Anal.* **47** 3671–86

[12] Shvydkoy R and Tadmor E 2017 Eulerian dynamics with a commutator forcing *Trans. Math. Appl.* **1** tnx001

[13] Do T, Kiselev A, Ryzhik L and Tan C 2018 Global regularity for the fractional Euler alignment system *Arch. Ration. Mech. Anal.* **228** 1–37

[14] Vicsek Tas, Czirók Aas, Ben-Jacob E, Cohen I and Shochet O 1995 Novel type of phase transition in a system of self-driven particles *Phys. Rev. Lett.* **75** 1226

[15] Shu R and Tadmor E 2020 Flocking hydrodynamics with external potentials *Arch. Ration. Mech. Anal.* **238** 347–81

[16] Reynolds C W 1987 Flocks, herds and schools: a distributed behavioral model *Proc. 14th Annual Conf. on Computer Graphics and Interactive Techniques* pp 25–34

[17] Vicsek Tas and Zafeiris A 2012 Collective motion *Phys. Rep.* **517** 71–140

[18] Cristina Marchetti M, Joanny J F, Ramaswamy S, Liverpool T B, Prost J, Rao M and Aditi Simha R 2013 Hydrodynamics of soft active matter *Rev. Mod. Phys.* **85** 1143

[19] Graner F and Riveline D 2017 'The forms of tissues, or cell-aggregates': D'arcy Thompson's influence and its limits *Development* **144** 4226–37

[20] Toyoda T, Mae S-I, Tanaka H, Kondo Y, Funato M, Hosokawa Y, Sudo T, Kawaguchi Y and Osafune K 2015 Cell aggregation optimizes the differentiation of human ESCs and iPSCs into pancreatic bud-like progenitor cells *Stem Cell Res.* **14** 185–97

[21] Zhang X, Xu L-H and Yu Q 2010 Cell aggregation induces phosphorylation of PECAM-1 and Pyk2 and promotes tumor cell anchorage-independent growth *Mol. Cancer* **9** 1–11

[22] Bayoussef Z, Dixon J E, Stolnik S and Shakesheff K M 2012 Aggregation promotes cell viability, proliferation and differentiation in an in vitro model of injection cell therapy *J. Tissue Eng. Regen. Med.* **6** e61–73

[23] Glinel K, Thebault P, Humblot V, Pradier C M and Jouenne T 2012 Antibacterial surfaces developed from bio-inspired approaches *Acta Biomater.* **8** 1670–84

[24] Green S K, Frankel A and Kerbel R S 1999 Adhesion-dependent multicellular drug resistance *Anti-Cancer Drug Des.* **14** 153–68

[25] St Croix B S and Kerbel R S 1997 Cell adhesion and drug resistance in cancer *Curr. Opin. Oncol.* **9** 549–56

[26] Brown J S, Cunningham J J and Gatenby R A 2016 Aggregation effects and population-based dynamics as a source of therapy resistance in cancer *IEEE Trans. Biomed. Eng.* **64** 512–8

[27] Lavi O, Greene J M, Levy D and Gottesman M M 2013 The role of cell density and intratumoral heterogeneity in multidrug resistancemodeling the intratumoral heterogeneity in multidrug resistance *Cancer Res.* **73** 7168–75

[28] Friedl P and Gilmour D 2009 Collective cell migration in morphogenesis, regeneration and cancer *Nat. Rev. Mol. Cell Biol.* **10** 445–57

[29] Theveneau E and Mayor R 2012 Neural crest migration: interplay between chemorepellents, chemoattractants, contact inhibition, epithelial–mesenchymal transition and collective cell migration *Wiley Interdiscip. Rev.: Dev. Biol.* **1** 435–45

[30] Varuni P, Menon S N and Menon G I 2017 Phototaxis as a collective phenomenon in cyanobacterial colonies *Sci. Rep.* **7** 1–10

[31] Morrell L J and James R 2008 Mechanisms for aggregation in animals: rule success depends on ecological variables *Behav. Ecol.* **19** 193–201

[32] Couzin I D, Krause J, James R, Ruxton G D and Franks N R 2002 Collective memory and spatial sorting in animal groups *J. Theor. Biol.* **218** 1–11

[33] Couzin I D and Franks N R 2003 Self-organized lane formation and optimized traffic flow in army ants *Proc. R. Soc.* B **270** 139–46

[34] Motsch S and Tadmor E 2011 A new model for self-organized dynamics and its flocking behavior *J. Stat. Phys.* **144** 923–47

[35] Conradt L and Roper T J 2005 Consensus decision making in animals *Trends Ecol. Evol.* **20** 449–56

[36] Krause J, Hoare D J, Croft D, Lawrence J, Ward A, Ruxton G D, Godin J J and James R 2000 Fish shoal composition: mechanisms and constraints *Proc. R. Soc.* B **267** 2011–7

[37] Hemelrijk C K, Reid D A P, Hildenbrandt H and Padding J T 2015 The increased efficiency of fish swimming in a school *Fish Fish.* **16** 511–21

[38] Marras S, Killen S S, Lindström J, McKenzie D J, Steffensen J F and Domenici P 2015 Fish swimming in schools save energy regardless of their spatial position *Behav. Ecol. Sociobiol.* **69** 219–26

[39] Cavagna A, Giardina I, Orlandi A, Parisi G, Procaccini A, Viale M and Zdravkovic V 2008 The starflag handbook on collective animal behaviour: part I, empirical methods (arXiv:0802.1668)

[40] Ballerini M *et al* 2008 Empirical investigation of starling flocks: a benchmark study in collective animal behaviour *Animal Behav.* **76** 201–15

[41] Lebar Bajec I L and Heppner F H 2009 Organized flight in birds *Animal Behav.* **78** 777–89

[42] Ling H, Mclvor G E, van der Vaart K, Vaughan R T, Thornton A and Ouellette N T 2019 Local interactions and their group-level consequences in flocking jackdaws *Proc. R. Soc.* B **286** 20190865

[43] Hughey L F, Hein A M, Strandburg-Peshkin A and Jensen F H 2018 Challenges and solutions for studying collective animal behaviour in the wild *Phil. Trans. R. Soc.* B **373** 20170005

[44] Goodenough A E, Little N, Carpenter W S, Hart A G and Hemelrijk C K 2017 Birds of a feather flock together: insights into starling murmuration behaviour revealed using citizen science *PLoS One* **12** e0179277

[45] Mueller T, O'Hara R B, Converse S J, Urbanek R P and Fagan W F 2013 Social learning of migratory performance *Science* **341** 999–1002
[46] Riters L V, Kelm-Nelson C A and Spool J A 2019 Why do birds flock? A role for opioids in the reinforcement of gregarious social interactions *Front. Physiol.* **10** 421
[47] Sarfati R, Hayes J C and Peleg O 2021 Self-organization in natural swarms of *Photinus carolinus* synchronous fireflies *Sci. Adv.* **7** eabg9259
[48] Buck J 1988 Synchronous rhythmic flashing of fireflies. II *Q. Rev. Biol.* **63** 265–89
[49] Penn Y, Segal M and Moses E 2016 Network synchronization in hippocampal neurons *Proc. Natl Acad. Sci.* **113** 3341–6
[50] Ben-Naim E 2005 Opinion dynamics: rise and fall of political parties *Europhys. Lett.* **69** 671
[51] Vicsek T 2001 A question of scale *Nature* **411** 421
[52] Delgado-Mata C, Ibanez Martinez J, Bee S, Ruiz-Rodarte R and Aylett R 2007 On the use of virtual animals with artificial fear in virtual environments *New Gener. Comput.* **25** 145–69
[53] Braga R G, Da Silva R C, Ramos A C B and Mora-Camino F 2018 Collision avoidance based on Reynolds rules: a case study using quadrotors *Information Technology-New Generations: 14th Int. Conf. on Information Technology* (Springer) pp 773–80
[54] Kennedy J and Eberhart R 1995 Particle swarm optimization *Proc. ICNN 1995-Int. Conf. on Neural Networks* vol 4 (IEEE) pp 1942–8
[55] Hartman C and Benes B 2006 Autonomous boids *Comput. Animat. Virtual Worlds* **17** 199–206
[56] Shu R and Tadmor E 2021 Anticipation breeds alignment *Arch. Ration. Mech. Anal.* **240** 203–41
[57] Carrillo Je A, D'Orsogna M R and Panferov V 2009 Double milling in self-propelled swarms from kinetic theory *Kinetic Relat. Models* **2** 363–78
[58] Ariel G and Ayali A 2015 Locust collective motion and its modeling *PLoS Comput. Biol.* **11** e1004522
[59] Buhl J, Sumpter D J T, Couzin I D, Hale J J, Despland E, Miller E R and Simpson S J 2006 From disorder to order in marching locusts *Science* **312** 1402–6
[60] Wilson S G 2004 Basking sharks (*Cetorhinus maximus*) schooling in the southern Gulf of Maine *Fish. Oceanogr.* **13** 283–6
[61] Malet-Engra G, Yu W, Oldani A, Rey-Barroso J, Gov Nir S, Scita G and Dupré Lıc 2015 Collective cell motility promotes chemotactic prowess and resistance to chemorepulsion *Curr. Biol.* **25** 242–50
[62] Copenhagen K, Malet-Engra G, Yu W, Scita G, Gov N and Gopinathan A 2018 Frustration-induced phases in migrating cell clusters *Sci. Adv.* **4** eaar8483
[63] Schneirla T C 1944 A unique case of circular milling in ants, considered in relation to trail following and the general problem of orientation *Am. Mus. Novit.* no. 1253
[64] Antoniou P, Pitsillides A, Blackwell T, Engelbrecht A and Michael L 2013 Congestion control in wireless sensor networks based on bird flocking behavior *Comput. Netw.* **57** 1167–91
[65] Hajihassani M, Jahed Armaghani D and Kalatehjari R 2018 Applications of particle swarm optimization in geotechnical engineering: a comprehensive review *Geotech. Geol. Eng.* **36** 705–22
[66] Vásárhelyi G, Virágh C, Somorjai G, Nepusz T, Eiben A E and Vicsek T 2018 Optimized flocking of autonomous drones in confined environments *Sci. Robot.* **3** eaat3536
[67] Cao Y, Yu W, Ren W and Chen G 2012 An overview of recent progress in the study of distributed multi-agent coordination *IEEE Trans. Ind. Inform.* **9** 427–38
[68] Olfati-Saber R 2006 Flocking for multi-agent dynamic systems: algorithms and theory *IEEE Trans. Autom. Control* **51** 401–20
[69] Vedel S, Tay S, Johnston D M, Bruus H and Quake S R 2013 Migration of cells in a social context *Proc. Natl Acad. Sci. USA* **110** 129–34
[70] Qin L, Yang D, Yi W, Cao H and Xiao G 2021 Roles of leader and follower cells in collective cell migration *Mol. Biol. Cell* **32** 1267–72
[71] Brian M V 2012 *Social Insects: Ecology and Behavioural Biology* (Dordrecht: Springer)
[72] Clutton-Brock T 2016 *Mammal Societies* (New York: Wiley)
[73] Alexandre G 2015 Chemotaxis control of transient cell aggregation *J. Bacteriol.* **197** 3230–7
[74] Chau R M W, Bhaya D and Casey Huang K C 2017 Emergent phototactic responses of cyanobacteria under complex light regimes *mBio* **8** e02330–16
[75] Ursell T, Man Wah Chau R, Wisen S, Bhaya D, Casey Huang K C and Haugh J M 2013 Motility enhancement through surface modification is sufficient for cyanobacterial community organization during phototaxis *PLoS Comput. Biol.* **9** e1003205
[76] Poujade M, Erwan Grasland-Mongrain E, Hertzog A, Jouanneau J, Chavrier P, Ladoux B, Buguin A and Silberzan P 2007 Collective migration of an epithelial monolayer in response to a model wound *Proc. Natl Acad. Sci. USA* **104** 15988–93
[77] Gov N S 2007 Collective cell migration patterns: follow the leader *Proc. Natl Acad. Sci. USA* **104** 15970–1
[78] Ladoux B and Mege R-M 2017 Mechanobiology of collective cell behaviours *Nat. Rev. Mol. Cell Biol.* **18** 743–57
[79] SenGupta S, Parent C A and Bear J E 2021 The principles of directed cell migration *Nat. Rev. Mol. Cell Biol.* **22** 529–47
[80] Czaczkes T J, Grüter C and Ratnieks F L W 2015 Trail pheromones: an integrative view of their role in social insect colony organization *Annu. Rev. Entomol.* **60** 581–99
[81] Perna A, Granovskiy B, Garnier S, Nicolis S C, Labédan M, Theraulaz G, Fourcassié V, Sumpter D J T and Ermentrout B 2012 Individual rules for trail pattern formation in argentine ants (*Linepithema humile*) *PLoS Comput. Biol.* **8** e1002592
[82] Gordon D M *et al* 2019 The ecology of collective behavior in ants *Annu. Rev. Entomol.* **64** 35–50
[83] Feinerman O, Pinkoviezky I, Gelblum A, Fonio E and Gov N S 2018 The physics of cooperative transport in groups of ants *Nat. Phys.* **14** 683–93
[84] Theveneau E and Linker C 2017 Leaders in collective migration: are front cells really endowed with a particular set of skills? *F1000 Res.* **6** 1899
[85] Kozyrska K, Pilia G, Vishwakarma M, Wagstaff L, Goschorska M, Cirillo S, Mohamad S, Gallacher K, Carazo Salas R E and Piddini E 2022 p53 directs leader cell behavior, migration and clearance during epithelial repair *Science* **375** eabl8876
[86] Bullo F 2019 *Lectures on Network Systems* vol 1 (Santa Barbara, CA: Kindle Direct Publishing)
[87] Levine H, Rappel W-J and Cohen I 2000 Self-organization in systems of self-propelled particles *Phys. Rev.* E **63** 017101
[88] D'Orsogna M R, Chuang Y L, Bertozzi A L and Chayes L S 2006 Self-propelled particles with soft-core interactions: patterns, stability and collapse *Phys. Rev. Lett.* **96** 104302
[89] Chaté H, Ginelli F, Grégoire G and Raynaud F 2008 Collective motion of self-propelled particles interacting without cohesion *Phys. Rev.* E **77** 046113
[90] Chuang Y-L, D'orsogna M R, Marthaler D, Bertozzi A L and Chayes L S 2007 State transitions and the continuum limit for a 2D interacting, self-propelled particle system *Physica* D **232** 33–47
[91] Minakowski P, Mucha P B, Peszek J and Zatorska E 2019 Singular Cucker–Smale dynamics *Active Particles* vol 2 (Berlin: Springer) pp 201–43
[92] Choi Y-P, Kalise D, Peszek J and Peters A A 2019 A collisionless singular Cucker–Smale model with decentralized formation control *SIAM J. Appl. Dyn. Syst.* **18** 1954–81

[93] Carrillo J A, Fornasier M, Rosado J and Toscani G 2010 Asymptotic flocking dynamics for the kinetic Cucker–Smale model *SIAM J. Math. Anal.* **42** 218–36
[94] Carrillo J A, Fornasier M, Toscani G and Vecil F 2010 Particle, kinetic and hydrodynamic models of swarming *Mathematical Modeling of Collective Behavior in Socio-Economic and Life Sciences* (Boston, MA: Birkhäuser) pp 297–336
[95] Carrillo J A, Choi Y-P and Hauray M 2014 The derivation of swarming models: mean-field limit and Wasserstein distances *Collective Dynamics From Bacteria to Crowds* vol 553 (Vienna: Springer) pp 1–46
[96] Choi Y-P, Ha S-Y and Li Z 2017 Emergent dynamics of the Cucker–Smale flocking model and its variants *Active Particles, Volume 1: Advances in Theory, Models and Applications* (Cham: Birkhäuser) pp 299–331
[97] Park J, Kim H J and Ha S-Y 2010 Cucker–Smale flocking with inter-particle bonding forces *IEEE Trans. Autom. Control* **55** 2617–23
[98] Djokam G A and Rathinam M 2022 A generalized model of flocking with steering *SIAM J. Appl. Dyn. Syst.* **21** 1352–81
[99] Ha S-Y and Liu J-G 2009 A simple proof of the Cucker–Smale flocking dynamics and mean-field limit *Commun. Math. Sci.* **7** 453–69
[100] Galante A, Wisen S, Bhaya D and Levy D 2011 Stochastic models and simulations of phototaxis *Unifying Themes Complex Syst.* **8** 105–19
[101] Ha S-Y and Levy D 2009 Particle, kinetic and fluid models for phototaxis *Discrete Contin. Dyn. Syst. Ser.* B **12** 77–108
[102] Bhaya D, Levy D and Requeijo T 2008 Group dynamics of phototaxis: interacting stochastic many-particle systems and their continuum limit *Hyperbolic Problems: Theory, Numerics, Applications* (Berlin: Springer) pp 145–59
[103] Levy D and Requeijo T 2008 Modeling group dynamics of phototaxis: from particle systems to PDEs *Discrete Contin. Dyn. Syst. Ser.* B **9** 103
[104] Levy D and Requeijo T 2008 Stochastic models for phototaxis *Bull. Math. Biol.* **70** 1684–706
[105] Risser D D and Meeks J C 2013 Comparative transcriptomics with a motility-deficient mutant leads to identification of a novel polysaccharide secretion system in *Nostoc punctiforme Mol. Microbiol.* **87** 884–93
[106] Menon S N, Varuni P, Menon G I and Rao C V 2020 Information integration and collective motility in phototactic cyanobacteria *PLoS Comput. Biol.* **16** e1007807
[107] Ben Amar M 2016 Collective chemotaxis and segregation of active bacterial colonies *Sci. Rep.* **6** 21269
[108] Keller E F and Segel L A 1971 Model for chemotaxis *J. Theor. Biol.* **30** 225–34
[109] Keller E F and Segel L A 1971 Traveling bands of chemotactic bacteria: a theoretical analysis *J. Theor. Biol.* **30** 235–48
[110] Alert R, Martínez-Calvo A and Datta S S 2022 Cellular sensing governs the stability of chemotactic fronts *Phys. Rev. Lett.* **128** 148101
[111] Shen J 2008 Cucker–Smale flocking under hierarchical leadership *SIAM J. Appl. Math.* **68** 694–719
[112] Shao J, Xing Zheng W X, Huang T-Z and Bishop A N 2018 On leader–follower consensus with switching topologies: an analysis inspired by pigeon hierarchies *IEEE Trans. Autom. Control* **63** 3588–93
[113] Aureli M and Porfiri M 2010 Coordination of self-propelled particles through external leadership *Europhys. Lett.* **92** 40004
[114] Mark S, Shlomovitz R, Gov N S, Poujade M, Grasland-Mongrain E and Silberzan P 2010 Physical model of the dynamic instability in an expanding cell culture *Biophys J.* **98** 361–70
[115] Tarle V, Ravasio A, Hakim V and Gov Nir S 2015 Modeling the finger instability in an expanding cell monolayer *Integr. Biol.* **7** 1218–27
[116] Tarle V, Gauquelin E, Ram Krishna Vedula S R K, d'Alessandro J, Lim C T, Ladoux B and Gov N S 2017 Modeling collective cell migration in geometric confinement *Phys. Biol.* **14** 035001
[117] Schuergers N, Lenn T, Kampmann R, Meissner M V, Esteves T, Temerinac-Ott M, Korvink J G, Lowe A R, Mullineaux C W and Wilde A 2016 Cyanobacteria use micro-optics to sense light direction *eLife* **5** e12620
[118] Chernetsov N, Pakhomov A, Kobylkov D, Kishkinev D, Holland R A and Mouritsen H 2017 Migratory Eurasian reed warblers can use magnetic declination to solve the longitude problem *Curr. Biol.* **27** 2647–51